



Lead-free potassium sodium niobate piezoceramics for high-power ultrasonic cutting application: Modelling and prototyping

Erdem Akça^{1,2,*}, Hüseyin Yılmaz²

¹Sivas Cumhuriyet University, Faculty of Engineering, Department of Metallurgical & Materials Engineering, 58140, Sivas, Turkey

²Gebze Technical University, Faculty of Engineering, Department of Materials Science & Engineering, 41400, Kocaeli, Turkey

Received 13 July 2018; Received in revised form 26 November 2018; Accepted 8 February 2019

Abstract

The motivation of this study was design, fabrication and characterization of bolt-clamped Langevin type transducers (BLT) from lead-free $K_{0.5}Na_{0.5}NbO_3$ (KNN) based piezoceramics for high-power ultrasonic cutting applications. Hard and lead-free KNN piezoceramics was obtained by adding $K_4CuNb_8O_{23}$ (KCN) together with ZnO and SnO_2 . Densification and high-power characteristics of KNN-KCN piezoceramics were enhanced in the presence of ZnO and SnO_2 . BLTs made from hard PZT4 (commercial $Pb(Zr,Ti)O_3$) or Zn,Sn co-doped KNN-KCN piezoceramic rings (KNN-KCN-ZnSn) were modelled through ATILA finite element analysis software package. Simulated and experimentally measured impedance spectra, resonance modes and harmonic analysis results of BLTs were compared with each other. Longitudinal vibration displacement at the tip of the horns of BLTs at approximately 30 kHz was measured via photonic sensor device to compare their performances. At the end, based on the simulation and experimental results, a prototype ultrasonic cutting device was fabricated from lead-free KNN-KCN-ZnSn piezoceramic rings. Its cutting action on both plastic and ceramic materials was demonstrated for the first time. In summary, it was found that a hard KNN-KCN based lead-free piezoceramics were good potential replacements for their lead-based counterparts for commercial high-power BLT applications.

Keywords: lead-free KNN piezoceramics, properties, BLT prototype device, modelling, application

I. Introduction

Piezoelectric materials have been widely used in various military and non-military applications in today's modern world. Smart materials exhibiting piezoelectric effect are, therefore, demanded in many areas like informatics, communication, transportation, energy, medicine etc. as sensors, actuators, generators and transducers [1–3]. It was estimated that global market size for piezoelectric devices should have reached ~38 billion US dollars in 2017 [3]. Furthermore, the market have been dominated mainly by lead based $Pb(Zr_xTi_{1-x})O_3$ (abbreviated as PZT) piezoceramics since the 1960s [1,3]. As a matter of fact, compositionally modified PZT based ceramics have superior electrical and electromechanical properties that are crucial in making var-

ious products. However, owing to the toxicity of lead for public health and environment, replacing lead-based piezoceramics with their lead-free counterparts have been encouraged. Especially, The EU's Restriction of Hazardous Substances (RoHS) Directive in 2003, which was later updated in 2011, has encouraged research activities on lead-free piezoceramics [4]. Eventually, the efforts bore fruit and in 2004 Saito *et al.* [5] announced one of the most promising lead-free piezoceramic candidates exhibiting comparable electromechanical properties to those of the lead-based counterparts made from $(K_{1-x}Na_x)NbO_3$ (abbreviated as KNN for $x = 0.5$). This breakthrough achievement drew researchers' attention and the recent studies have been mainly focused on the development of new lead-free piezoceramics. However, it is as equally important to put the research outcome into use for society's benefit. According to Rödel *et al.* [1] vision, published in 2015, researches on appli-

*Corresponding author: tel: +90 346 2191010 Ext. 2808, e-mail: erdemakca@cumhuriyet.edu.tr

cation oriented developments of lead-free piezoceramics would dominate the researches on lead-free piezoceramics by the 2020s.

The first commercial lead-free piezoceramic transducer was marketed by Honda Electronics (relevant paper published in 2009 [6]) as bolt-clamped Langevin type transducer (BLT) for ultrasonic cleaning application. BLTs are typical high-power ultrasonic applications of transducers and basically consist of two or more ring shaped piezoelectric materials sandwiched between a back mass and a front mass by a pre-stressed screw bolt. BLTs, which are usually operated in the frequency range from 20 to 100 kHz, have been currently used in areas where high ultrasonic vibrations are required [7,8]. Ultrasonic cleaning, cutting, drilling, welding, forming, machining and sonochemistry are some common examples where BLTs are regularly employed [8–16]. Usually, Navy type I (PZT4) and Navy type III (PZT8) piezoceramic rings exhibiting hard character are the first choice as active elements in commercial BLTs because of their low mechanical and electrical losses. Although several promising lead-free piezoceramics have been developed since 2000s, hard PZT piezoceramics still dominate studies on BLTs for high-power ultrasonic applications [9,11,15–19]. Unfortunately, there were very few studies on the application of BLTs for ultrasonic devices made from eco-friendly lead-free piezoceramics in literature [6,20–24]. In the relevant rare studies, modified KNN or (Na,Bi)TiO₃ (NBT) based piezoceramics were used for ultrasonic cleaning or ultrasonic wire-bonding applications. However, the piezoceramics in most of those studies [20–22,24] may not be the best choices among the candidates for high-power application, except the ones in the study of Tou *et al.* [6]. In most of these studies, the piezoceramics exhibited a low mechanical quality factor (Q_m) between 80 and 140 and a high dielectric loss ($\tan \delta$) at about ~2%, resembling soft type piezoceramics, which are usually not good enough in making BLTs [20–22,24]. It is known that the widely used lead-based hard piezoceramics, such as PZT4 and PZT8, in most of the high-power ultrasonic applications possess a high Q_m (500–1000) and a low $\tan \delta$ (0.4–0.6%) [25,26]. Piezoelectric ceramics for high-power applications should have low electrical ($\tan \delta$) and mechanical losses ($\tan \delta_m = 1/Q_m$) in order to minimize the power dissipation which results in the internal heating during operation [25]. The rise in the temperature due to these losses may be detrimental to the device or restricts its use extensively. The need for a hard lead-free piezoceramic which have comparable electrical and electromechanical properties to those of lead-based hard PZTs still continues [1,25,27–29].

In this study, an ultrasonic cutting device, which is a typical high-power application of BLT, was made from hard KNN-based piezoceramics. It is well known that the main drawback in the uses of KNN as a piezoceramics is its poor electrical reproducibility associated

with its poor sinterability in the pure form. That is why KNN piezoceramics were sintered with additives (or dopants) to overcome abovementioned problems. Additives such as CuO, ZnO, SnO₂, Li₂O, MnO₂, V₂O₅, GeO₂ and SrCO₃ were reported to promote densification in KNN piezoceramics [30–39]. The hard character of piezoceramics with perovskite structure is induced via A-site or B-site acceptor doping, by “pinning” the domain walls [29,40]. However, some of the additives such as CuO and K₄CuNb₈O₂₃ (the latter one is abbreviated as KCN), not only enhance densification but also induce hard character within KNN piezoceramics [26,33,38,41–52]. Processing, microstructure, hardening mechanism, thermal stability as well as piezoelectric, dielectric and elastic properties of KCN modified KNN based piezoceramics were reported previously [26,46–48,52–64]. Isothermal and dynamic sintering kinetic studies, and electrical and electromechanical characterizations of doped KNN-KCN piezoceramics as well as making of an ultrasonic cutter and homogenizer from these piezoceramics were done by Akça [65]. The effects of various oxide addition on sintering behaviour and electrical properties of eco-friendly hard KNN-KCN piezoceramics were studied in our previous work [66]. It was found that especially addition of ZnO and SnO₂ enhanced densification of KNN-KCN piezoceramics by lowering the sintering temperature by 40 °C without deteriorating dielectric and piezoelectric properties as well as its hard character [66].

In the current study, the effect of ZnO and SnO₂ addition on the electrical and electromechanical properties of KNN-KCN piezoceramics and their use as a transducer for a high-power ultrasonic application were reported. Fabrication and characterization of a prototype BLT type ultrasonic cutting device made from lead-free KNN piezoceramic rings were done as well.

II. Experimental

The raw materials for preparation of the undoped and Zn,Sn-doped KNN-KCN ceramics were K₂CO₃ (Merck, 99%), Na₂CO₃ (Merck, 99%), Nb₂O₅ (Alfa Aesar, 99.5%), ZnO (Sigma-Aldrich, 99%), SnO₂ (Alfa Aesar, 99.9%) and CuO (Merck, 96%). In the first step, intermediate powders K₄CuNb₈O₂₃ (KCN), K_{0.5}Na_{0.5}NbO₃ (KNN) and 0.8 mol% (Zn,Sn) co-doped K_{0.5}Na_{0.5}NbO₃ (KNN-ZnSn) were synthesized via mixed oxide route. K₂CO₃ and Na₂CO₃ were first kept in a drying oven at 200 °C for 24 h. Then, stoichiometric amounts of raw materials were weighed according to the chemical formulas and ball milled in a 125 ml high density polyethylene bottle by using anhydrous ethanol and 3–5 mm partially stabilized ZrO₂ balls at 140 rpm for 24 h. The obtained KCN and KNN powders were calcined in open alumina crucibles at 600 °C for 2 h and 700 °C for 2 h, respectively. The calcined powders were then ball milled for another 24 h and dried on a magnetic stirrer. KNN or KNN-ZnSn powders were mixed

with 0.5 mol% KCN together with polymeric binder solution consisting of ethanol, fish oil (Sigma-Aldrich), polyvinyl butyral (Sigma-Aldrich) and dioctyl phthalate (Sigma-Aldrich). The undoped and doped compositions were named as KNN-KCN and KNN-KCN-ZnSn, respectively. Green samples were uniaxially pressed in a 31.5 mm diameter steel mould at 100 MPa before the binder burn-out process by holding them at 275 °C for 1 h and at 600 °C for 1 h with 1 °C/min heating rate in between these holding temperatures. Then, KNN-KCN and KNN-KCN-ZnSn ceramics were sintered in the air atmosphere at 1120 °C for 2 h and 1080 °C for 2 h, respectively, at 5 °C/min heating and 10 °C/min cooling rates. In order to compensate for the possible weight loss due to possible alkali volatilization, the samples were sintered in KNN powder bed. Densities of the sintered samples were measured by the Archimedes' technique. The standard deviation in densities was calculated at least from five different samples.

Full set of electromechanical coefficients of poled KNN piezoceramics (∞ m Curie group) were basically measured in accordance with the method set out in the IEEE standards on piezoelectricity [67]. Besides, the shear mode coefficients were measured by using length shear vibrators [68]. The parallel surfaces of the sintered discs were polished using 1200-grit SiC paper. Samples with special geometry and dimensions were also cut by using precision cutting disc. The samples were electroded by silver paste and then baked in the air atmosphere at 600 °C for 30 min. Poling was done in a silicone oil at 120 °C for 15 min at 50 kV/cm before cooling the samples down to RT under electrical field. The piezoelectric charge coefficient (d_{33}) was measured 24 h after the poling process by using a Berlincourt d_{33} -meter (Sinocera, YE2730A). Meanwhile, the variation of dielectric constant ($\epsilon_{33}^T/\epsilon_0$), and planar coupling coefficient (k_p) as a function of temperature and the orthorhombic-tetragonal phase transition temperature ($T_{O \rightarrow T}$) of the poled ceramic disc were determined using LCR meter (Hioki, 3532-50).

Simulation studies were done using ATILA (version 6.0.0.6) finite element analysis (FEA) software with the GID (version 10.0.9) pre/postprocessor. ATILA is a commercially available FEA software package, which is specifically developed for the modelling and analysis of devices made from piezoelectric or magnetostrictive materials [69,70]. It was at this stage where optimum geometries and dimensions of all parts that make up a BLT were determined. Subsequently, the parts made from metal such as back masses and horns were manufactured with a maximum dimensional tolerance of 1% via universal lathe.

The longitudinal displacement on the tip of the horn of BLTs, at the working frequency, was measured by using a high resolution non-contact photonic sensor (MTI-2000) equipped with a high precision fiber-optic probe. In order to drive the BLT, a voltage with a sinusoidal waveform was first created by using a function genera-

tor (Rigol DG1022) which was later amplified through an amplifier (NF HSA-4052), and the response of BLT was monitored by the photonic sensor and recorded at the same time by an oscilloscope (Agilent D50-X 2024A).

III. Characterization of KNN-based ceramics

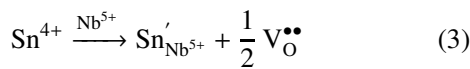
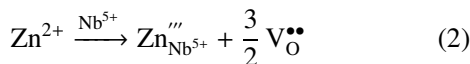
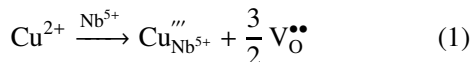
The optimum sintering temperature was found to be 1120 °C with a relative density of $98 \pm 0.2\%$ TD for the undoped KNN-KCN ceramics, whereas it was found to be 1080 °C with a relative density of $99 \pm 0.2\%$ TD for Zn,Sn co-doped ones. A decrease in the optimum sintering temperature of KNN-KCN by 40 °C was attributed to the eutectic reaction between ZnO and KCN. It is a well-known fact that copper oxide based additives, such as CuO or KCN, play important role in improving sinterability of KNN by liquid phase formation [60,61]. However, doping or co-doping with Zn^{2+} , Sn^{4+} , $Zn^{2+}Sn^{4+}$, $Zn^{2+}Cu^{2+}$ or $Sn^{4+}Cu^{2+}$, were also reported to enhance the densification of KNN ceramics [32,34,39,71]. In previous works, the addition of ZnO into Cu-doped KNN ceramics was stated to result in the formation of liquid phase at lower temperatures due to the eutectic reaction between ZnO and CuO [34]. Moreover, the incorporation of Zn^{2+} ions into the Cu-rich secondary phase accumulated at the grain boundaries, was confirmed by energy-dispersive spectroscopy (EDS) analysis [34]. In another study, the density of KCN doped ($K_{0.5}Na_{0.5})(Nb_{0.94}Sb_{0.04})O_3$ ceramics was found to increase with ZnO addition up to 0.8 mol% ZnO addition [62]. However, Sn-doping promoted densification of KNN ceramics by inhibiting the grain growth/coarsening, unlike Zn^{2+} and/or Cu^{2+} doped ones [39]. Since piezoceramics with larger grain sizes are not desired, Sn-doping was used to prevent the abnormal grain growth in Zn-doped KNN-KCN ceramics. Therefore, it was concluded that the eutectic reaction between ZnO and KCN and the prevention of abnormal grain growth by Sn-doping were responsible for the improvement in the sintered densities and reproducibility in KNN-KCN ceramics as compared to the undoped ones in wide sintering temperatures [66]. Moreover, small peaks from KCN were detected in the XRD patterns (not shown here) of KNN-KCN and KNN-KCN-ZnSn ceramics sintered at their optimum sintering temperatures. However, KCN phase was not observed in microstructures as mentioned in our previous work. Matsubara *et al.* [60] also reported the presence of uniformly distributed Cu ions throughout the microstructure despite detectable KCN phase in XRD pattern in the presence of 0.5 mol% KCN.

The non-zero and independent elasto-piezo-dielectric coefficients of the undoped and Zn,Sn-doped KNN-KCN piezoceramics sintered at their optimum sintering temperatures are given in Table 1. A low dielectric loss ($\tan \delta$) together with a high mechanical quality factor (Q_m) were one of the most important indications of a

Table 1. The elasto-piezo-dielectric coefficients of KNN-KCN based piezoceramics

	KNN-KCN	KNN-KCN-ZnSn
$\tan \delta$ [%]	0.6	0.35
Q_m	907	1300
$\epsilon_{33}^T/\epsilon_0$	340	325
$\epsilon_{11}^T/\epsilon_0$	465	454
d_{31} [pC/N]	-31	-33
d_{15} [pC/N]	114	115
d_{33} [pC/N]	89	94
s_{11}^E [$\mu\text{m}^2/\text{N}$]	7.69	7.6
s_{12}^E [$\mu\text{m}^2/\text{N}$]	-2.55	-2.34
s_{13}^E [$\mu\text{m}^2/\text{N}$]	-2	-2.18
s_{33}^E [$\mu\text{m}^2/\text{N}$]	8.8	9.72
s_{44}^E [$\mu\text{m}^2/\text{N}$]	20.3	19.8

hard character in piezoelectric materials. It was found that electrical losses ($\tan \delta$ measured at 1 kHz) and mechanical losses ($\tan \delta_m = Q_m^{-1}$) of the undoped KNN-KCN piezoceramics decreased dramatically with Zn,Sn co-doping. It is known that hardening of piezoelectric properties was directly associated with the formation of point defects with doping [29,72]. The ionic radii of K^+ , Na^+ , Nb^{5+} , Cu^{2+} , Zn^{2+} and Sn^{4+} are 164, 139, 64, 72, 74 and 69 pm, respectively [73]. It is believed that Cu^{2+} , Zn^{2+} and Sn^{4+} ions can occupy the B-sites in perovskite lattice due to their similar ionic radii as the Nb^{5+} ion. The probable defect formation reactions, using the Kröger-Vink notations, describing the incorporation of Cu^{2+} , Zn^{2+} or Sn^{4+} ions into the KNN unit cell, are shown in Eqs. 1-3.



The hard character in the KNN piezoceramics is caused by the formation of oxygen vacancies ($\text{V}_{\text{O}}^{\bullet\bullet}$) due to the Cu^{2+} ion substitution into the Nb^{5+} site, as shown in Eq. 1 [74–78]. Moreover, the substitution of Zn^{2+} and Sn^{4+} ions for Nb^{5+} into the B-site of the perovskite structure probably further increased the concentration of oxygen vacancy defects, $[\text{V}_{\text{O}}^{\bullet\bullet}]$. The increase in the $[\text{V}_{\text{O}}^{\bullet\bullet}]$ concentration with Zn^{2+} and Sn^{4+} ion doping, highly likely contributed to the hard character by reducing the domain wall mobility and therefore domain switching in KNN piezoceramics due to the so called “pinning effect” [62,71]. Also, dielectric constants ($\epsilon_{33}^T/\epsilon_0$ and $\epsilon_{11}^T/\epsilon_0$) were found to decrease with Zn,Sn co-doping confirming hardening in piezoelectric properties. However, any considerable change in the piezoelectric charge coefficients (d_{31} , d_{15} and d_{33})

and elastic compliances (s_{ij}^E) were not observed with the co-doping. There are intrinsic and extrinsic contributions to the overall dielectric, piezoelectric and electromechanical properties. While the intrinsic contributions are related to the ions in the crystal lattice, extrinsic contributions come from domain wall vibration, domain wall motion and domain switching [79,80]. In order to understand how dielectric, piezoelectric and elastic properties of KNN-KCN based piezoceramics change, both the presence of the point defects and domain wall contributions have to be taken into account. Cu-doping, undoubtedly, affected the dynamics of the domain wall motion because it resulted in hard-type behaviour in KNN. In this study, it was assumed that Zn and Sn co-doping enhanced hard character in KNN-KCN piezoceramics by defect complex formations. The dielectric and piezoelectric properties of piezoceramics were expected to decrease as a result of the decrease in domain wall mobility due to the interaction of domain walls with oxygen vacancy involving defect complexes. As a matter of fact, lower dielectric constant, dielectric and mechanical losses were taken as the evidences of hardening in KNN-KCN with Zn,Sn co-doping. However, the piezoelectric and electromechanical properties of KNN-KCN piezoceramic did not decrease in the presence of Zn,Sn co-doping as expected. Therefore, the effect of other factors on the domain wall dynamics such as non-linear behaviour, poling efficiency and bias field of KNN-KCN based piezoceramics should be taken into consideration. Unfortunately, detailed experimental study about the domain configuration and domain dynamics that affect the intrinsic and extrinsic response of KNN-KCN based piezoceramics in literature is scarce.

Electromechanical coupling coefficients (k_p and k_{ij} : k_{31} , k_{15} , k_{33}), which are material parameters related to the conversion efficiency of electrical energy into mechanical energy or vice versa in piezoelectric materials, were measured as well. The longitudinal electromechanical coupling coefficients (k_{33}) were estimated from Eq. 4 [81]:

$$(k_{33})^2 \approx (k_p)^2 + (k_t)^2 - (k_p)^2 \cdot (k_t)^2 \quad (4)$$

Those coefficients were estimated as $k_p = 0.35$ and 0.39 , $k_{31} = 0.2$ and 0.23 , $k_{33} = 0.55$, $k_{15} = 0.44$ and 0.46 for the undoped and Zn,Sn co-doped KNN-KCN ceramics, respectively. However, just knowing the coupling coefficients (k_{ij}) was not enough for the evaluation of the efficiency of transduction, because the electrical and mechanical losses in a piezoceramics also play a crucial role in the performance of the transducer during operation. Therefore, the figure of merit of piezoceramics, defined as $k_{33}^2 \cdot Q_m$, is usually taken as a material selection criterion for high power ultrasonic applications for devices working at resonance frequencies i.e. sonar, ultrasonic cutter, piezoelectric transformer, accelerometer etc. [1,28,82]. In addition, other electrical and elec-

electromechanical coefficients, such as d_{ij} , ε_{33}^T , s_{ij}^E , which are interrelated to k_{ij} , must also be taken into account for the sake of a better material selection to be used in designing of a high-power ultrasonic device. Thereby, derived material parameters, such as acoustic power density (P_{aco}) and vibration velocity (v_0) as shown in Eqs. 5 and 6, were calculated to compare the high-power characteristics of piezoelectric materials [27,28]:

$$P_{aco} = 2\pi \cdot f_r \cdot E^2 \cdot k_{ij}^2 \cdot \varepsilon_{33}^T \cdot Q_m \quad (5)$$

$$v_0 = \frac{4}{\pi} \sqrt{\frac{\varepsilon_{33}^T}{\rho}} (k_{31} \cdot Q_m) \cdot E \quad (6)$$

where f_r is the resonance frequency and E is the driving electric field. For instance, higher P_{aco} and/or v_0 values mean that a higher power output could be obtained from the ultrasonic transducer working at resonance frequencies made from these materials. Table 2 compares the high-power characteristics of PZT4, KNN-KCN and KNN-KCN-ZnSn piezoceramics with each other, which were assumed to operate under identical conditions.

In these calculations non-linearities in the proper-

Table 2. Comparison of the high-power characteristics of lead-based and lead-free piezoceramics

Properties	PZT4	KNN-KCN	KNN-KCN-ZnSn
	Ref. [26]	This work	This work
d_{33} [pC/N]	289	89	94
k_{33}	0.7	0.55	0.55
k_{31}	0.33	0.2	0.23
$\varepsilon_{33}^T/\varepsilon_0$	1300	340	325
Q_m	500	907	1300
ρ [kg/m ³]	7600	4440	4450
f_r [Hz]	20000	20000	20000
E [V/m]	100	100	100
$k_{33}^2 \cdot Q_m$	245	274	393
P_{aco} [W/m ³]	3544	1038	1422
v_0 [mm/s]	26	19	31

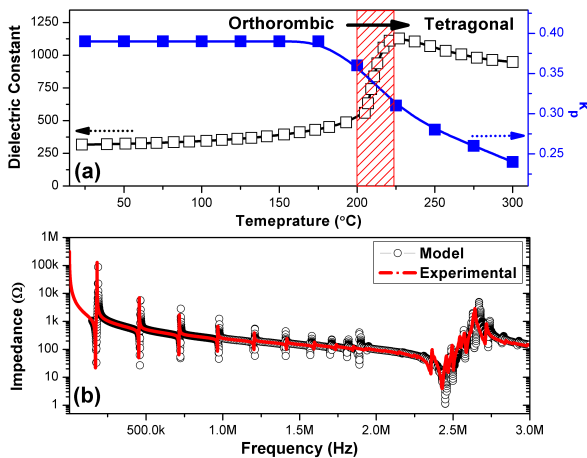


Figure 1. (a) k_p and dielectric constant of KNN-KCN-ZnSn ceramics as a function of temperature, (b) Comparison of simulated and experimentally measured impedance spectrums for KNN-KCN-ZnSn

ties of piezoceramics, usually seen when a certain electric field value was exceeded, were neglected [83]. A higher $k_{ij}^2 \cdot Q_m$ figure of merit value was obtained for KNN-KCN-ZnSn piezoceramics because of its higher Q_m value. Even though lead-based PZT4 piezoceramics seem to be a better candidate for a high-power ultrasonic application, due to their higher dielectric constants and, therefore, higher P_{aco} values, it is important that the piezoceramics possess a hard character to keep their electrical and mechanical losses ($\tan \delta$ and $\tan \delta_m$) low enough when driven under high electric fields, in other words, at high vibration velocities [84]. Lead-free hard Cu-doped KNN based and Mn-doped NBT based piezoceramics were reported to exhibit a better high-power performance as compared to hard PZTs [84,85]. Based on the calculated vibration velocity values given in Table 2, the high-power characteristic of the lead-free KNN-KCN-ZnSn ceramics was found to be comparable to that of lead-based PZT4. Moreover, electrical (P_{loss}) or mechanical (W_{loss}) losses may result in generation of heat in the piezoelectric materials during vibration at the resonance frequencies. These losses per unit volume were calculated using Eqs. 7 and 8:

$$P_{loss} = 2\pi \cdot f \cdot \varepsilon_{33}^T \cdot \tan \delta \cdot E^2 \quad (7)$$

$$W_{loss} = \pi \cdot f \cdot s_{ij}^E \cdot X^2 \cdot Q_m^{-1} \quad (8)$$

where X is the mechanical stress and f is the frequency. Piezoelectric ceramics dissipate energy in the form of heat which is proportional to $\varepsilon_{33}^T \cdot \tan \delta$ or s_{ij}^E/Q_m . Therefore, at identical frequency, stress and electric field values, the power losses in lead-free KNN-KCN based ceramics were much lower than those of lead-based PZT4. The power losses are critical during service because they may lead to a temperature rise in the device, which at the end may have a detrimental effect on the piezoelectric ceramics, like degradation of the electrical properties or even de-poling. Gradual or sharp increases in both dielectric constant and dielectric loss due to the temperature rise mainly originate from internal friction in a piezoceramics during operation. Hence, the dependence of dielectric properties on temperature has to be taken into account to make a device that has enough thermal stability within operating temperatures. It is known that KNN-KCN piezoceramics possess a better thermal stability as compared to hard PZT ones [26]. Figure 1a showed the variations of k_p and dielectric constant of KNN-KCN-ZnSn ceramics as a function of temperature between room temperature and 300 °C. Electromechanical properties of KNN-KCN-ZnSn were stable up to its orthorhombic to tetragonal phase transition temperature ($T_{O \rightarrow T} > 200$ °C) where a dielectric anomaly was observed. In other words, the safe operation temperature window of KNN-KCN-ZnSn was upper bound by its orthorhombic to tetragonal phase transition temperature. However, it is almost impossible for PZT4 ceramics to maintain their high electromechanical properties up to ~200 °C as KNN-KCN-ZnSn piezo-

ceramics [26]. Therefore, it is concluded that KNN-KCN-ZnSn piezoceramics obviously exhibit a better thermal stability and low power loss behaviour as compared to PZT4. It was found that Zn,Sn co-doping not only decreased the sintering temperature by 40 °C, but also made KNN-KCN piezoceramics better candidate for high-power ultrasonic applications [67]. Therefore, a Langevin type prototype device was fabricated from KNN-KCN-ZnSn piezoceramics to test its potential as a lead-free piezoelectric material for a high-power ultrasonic cutting application.

In Fig. 1b the modelled and experimentally measured impedance spectra of a poled KNN-KCN-ZnSn disc with standard geometry (diameter/thickness ratio ≈ 17) are compared with each other. The first peak in the spectrum corresponds to the fundamental radial mode vibrations with again radial harmonic overtones up to ~ 2 MHz. The second peak to the right corresponds to the fundamental thickness mode vibrations. These were the two main characteristic peaks observed in the impedance spectrum of a poled standard disc sample. The modelled and experimentally measured spectra were so much consistent with each other that the difference between both resonance and anti-resonance frequencies (f_r and f_a) either by simulation or experimental were lower than 3%. The compatibility of modelling and experimental results heavily depended on the accuracy of material input data required for FEA software. Therefore, it was crucial to have reproducible and reliable material parameters. The impedance spectrum was simulated from the measured electrical and electromechanical coefficients given in Table 1.

IV. Prototype device - modelling and fabrication

In this study, bolt clamped Langevin type ultrasonic cutting device operating at ~ 40 kHz working frequency was modelled in order to compare the effect of type of hard lead-based PZT and lead-free KNN-KCN based piezoceramics on the efficiency of longitudinal ultrasonic energy transfer from the transducer. The cross sectional view (one quarter) of a prototype ultrasonic

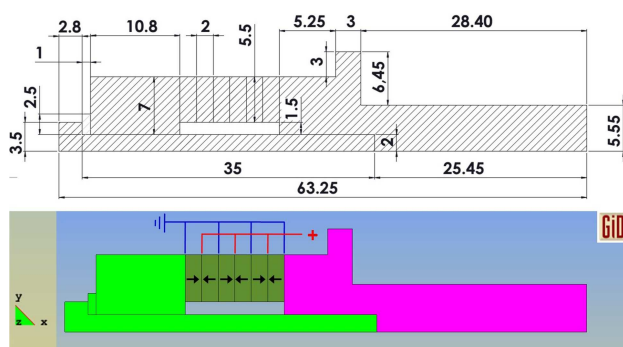


Figure 2. Cross sectional view (one quarter) of BLT with dimensions (light green: steel, dark green: lead-free or lead-based piezoceramics, pink: aluminium, red line: electrical force, navy line: electrical ground and the “arrows” indicate the polarization axis)

transducer design with its dimensions in millimetres is given in Fig. 2. The prototype device consisted of six-ring shaped piezoceramics sandwiched between a steel back mass and an aluminium front mass by a steel prestressed screw bolt. Meanwhile, high density steel back mass and low density aluminium front mass (horn) were used for the sake of efficient transfer of longitudinal ultrasonic energy from piezoelectric elements into the tip of horn. It was obvious that motion mainly in the x -direction at the tip of horn was desired for a good axial ultrasonic cutting process. Besides, in order to amplify the longitudinal displacement in the x -direction, the front mass was particularly designed as a stepped horn, since the gain was found to be proportional to the square of the input and output end diameter ratio of the horn [86].

The stepped horn was known to give the largest displacement amplification (high gain) among the horns, such as exponentially, conically, cantenoidal tapered or parametric curved horns [87]. Furthermore, the aluminium horn had a flange so that the transducer could be fixed. Those flanges were designed to be the nodal points during operation of the transducer. The outer and inner diameters of the 2 mm thick ceramic rings were 18 mm and 7 mm, respectively. The material properties used in simulation of the whole assembly (transducer) were as follows: elastic modulus, Poisson’s ratio and density for AISI/SAE 4140 steel were $Y = 210$ GPa, $\nu = 0.285$, $\rho = 7800$ kg/m³ and for 7075 aluminium were $Y = 71.4$ GPa, $\nu = 0.344$, $\rho = 2780$ kg/m³, respectively. Thin copper foils which were 100 μ m thick were used in the assembly but neglected during finite element modelling. The transducer design was optimized by systematically changing the design parameters, such as dimensions and number of ceramic rings, length of screw bolt and/or back mass etc. as shown in Fig. 2 [65]. Maximum displacement at the tip of the horn and maximum effective electromechanical coupling coefficient ($k_{eff} = (1 - (f_r/f_a)^2)^{1/2}$) of the transducer, were taken into account to design a transducer at 40 kHz working frequency (details are not shown here). The same design as given in Fig. 2 was used for making prototype ultrasonic transducers from lead-based PZT-4 piezoceramics (abbreviated as P-6) and lead-free KNN-KCN-ZnSn piezoceramics (abbreviated as K-6).

Impedance spectra of the transducers in the range from 1 to 100 kHz were simulated by FEA as shown in Fig. 3. Frequency intervals were 660 Hz for 1–100 kHz range and 40 Hz for 30–50 kHz range, respectively. In both designs three different resonance peaks were present in the spectra in the range from 1 to 100 kHz frequency. The first resonance peaks were found to be at 39.35 kHz and 37.25 kHz for K-6 and P-6 transducers, respectively, which were known as the fundamental resonance frequencies (f_r). It is confirmed by harmonic analysis that the resonance peaks observed at higher frequencies between 60–70 kHz and 90–95 kHz in both designs were mainly associated with fluttering of flange.

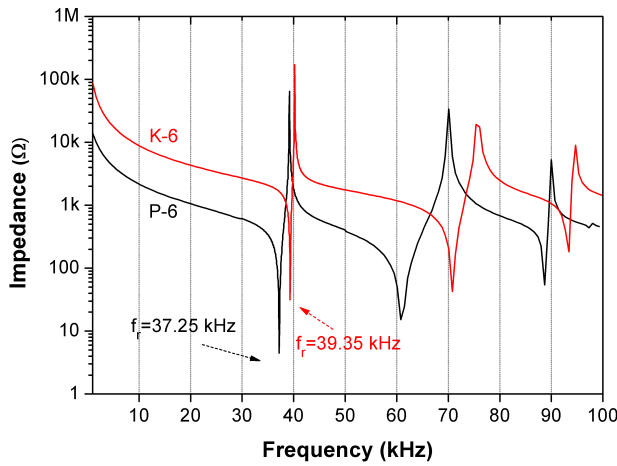


Figure 3. Simulated impedance spectra from 1 to 100 kHz for BLTs of K-6 and P-6

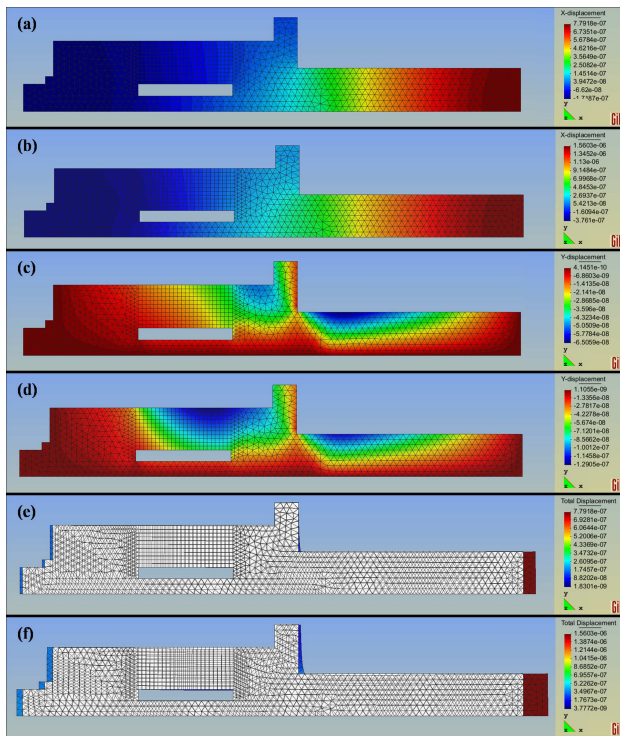


Figure 4. Displacement contour plots at fundamental resonance frequency; (a-b) in x -direction, (c-d) in y -direction and (e-f) total displacement mode shapes compared with original mesh for BLTs of K-6 and P-6, respectively

Figure 4 is given to compare the simulated displacement contour plots at fundamental resonance frequencies of K-6 and P-6 transducers. In Fig. 4a,b, dark red regions at the tip of the horns refer to maximum displacements in the positive x -direction, whereas navy regions at the end of back masses and head of screw bolts refer to maximum displacements in the negative x -direction. Displacement scales in the respective directions are shown on the right-side of the figures. Maximum displacements for transducers in the positive and negative x -directions were $0.78 \mu\text{m}$ and $-0.17 \mu\text{m}$ at the fundamental resonance frequency of $f_r = 39.35 \text{ kHz}$

(for K-6) and $1.56 \mu\text{m}$ and $-0.38 \mu\text{m}$ at the fundamental resonance frequency of $f_r = 37.25 \text{ kHz}$ (for P-6), respectively. These simulations were carried out assuming electrical potential difference of 1 V. The displacements in the positive x -direction for both transducers are approximately four times greater than those in the negative x -direction. In other words, the largest x -displacements are mainly observed at the tips of the horns, as wanted. In Fig. 4c,d, navy regions refer to maximum displacements in the negative y -direction while dark red regions refer to maximum displacements in the positive y -direction. Maximum displacements in the negative y -directions were $-0.065 \mu\text{m}$ and $-0.13 \mu\text{m}$ at fundamental resonance frequencies, f_r of K-6 and P-6 transducers, respectively. Moreover, the displacement values in the negative y -direction are much bigger than those in the positive y -directions. Besides, the ratio of maximum displacement in the x -direction to that in the y -direction is approximately between 10 and 12 for both transducers. Displacement in the x -direction was desired rather than any other directions for the sake of effective longitudinal cutting action. In Fig. 4e,f, total displacement mode shapes are compared with original meshes (shown as white colour) for K-6 and P-6 transducers driven at their respective fundamental frequencies f_r . Total displacement mode shapes observed mainly in the positive x -directions at the tips of the horns are a good indication of virtually pure longitudinal motion. Much lower displacements at the back mass and flange in comparison to the one at the tip of horn meant that the acoustic power due to the resonance vibration of piezoceramics was being transmitted effectively into the tips of the horn (in the x -direction) during the operation.

Meanwhile, the total displacement in P-6 transducer was higher than that of K-6 one as expected. Because k_{eff} values, which were related to energy transduction of transducers, were calculated from the simulated fundamental resonance peaks and were found to be 0.21 and 0.32 for K-6 and P-6, respectively. Owing to the two times bigger total displacements at the tips, P-6 transducer clearly have an advantage over K-6 one for the ultrasonic cutting process. However, superior thermal



Figure 5. Parts of Langevin type ultrasonic device before assembling (a), K-6 lead-free BLT (b), prototype ultrasonic cutting device including lead-free KNN-KCN-ZnSn piezoceramics (c)

stability and lower power loss characteristics of KNN-KCN based piezoceramics over those of hard PZT, make it a good alternative candidate to be used as piezoceramic in devices requiring long term use. In addition, higher displacement in the flange of P-6 transducers (Fig. 4f) may be a disadvantage which needs to be fixed during service. That is, dimensions given only by looking at the displacement at the tip of horn is not enough to state that PZT based P-6 transducer is more suitable than KNN based K-6 one for cutting applications. However, it would be more appropriate to study the thermal

stability of the KNN-KCN-ZnSn and PZT4 based transducers during service to see the overall advantage and which piezoceramics is more convenient.

The parts used in making a Langevin type ultrasonic device before assembling are shown in Fig. 5a. Two different types of horn were made. Bare horn which is the one used in modelling of the transducers as shown in Fig. 5b. The other is the holder horn with a stainless steel hobby blade attached to the vertical groove at the aluminium tip, which was used as the horn for cutting. The groove is 18 mm in length and 0.6 mm in width. There is a cylindrical relief about 2 mm in diameter at back end of the groove and a perpendicular M2.5 screw hole in the middle of the groove for clamping the blade. The prototype ultrasonic cutting device made of KNN-KCN-ZnSn piezoceramics is shown in Fig. 5c.

In Fig. 6, measured impedance-frequency spectra for K-6 and P-6 BLTs are compared with the simulated ones. The experimentally measured resonance and anti-resonance peaks of both BLTs were found to be at lower frequencies in comparison to that obtained by simulation. Measured and simulated fundamental resonance frequencies were 33.1 and 39.3 kHz for K-6 transducer, whereas they were 30 and 37.2 kHz for P-6 transducer, respectively. The differences in fundamental resonance frequencies were approximately 16% and 20% for K-6 and P-6 transducers, respectively. The agreement or disagreement between measured and simulated impedance spectra depends on several factors, e.g. dimensional tolerances in the ceramic and metal parts, consistency and reliability in full set of material parameters which were required for FEA and/or applied torque to pre-stress the bolt that holds the whole assembly together etc. Even though a torque has to be applied to a level at which the position and the intensity of the resonance and anti-resonance peaks become stationary, due to the cracking of piezoceramic rings a torque value of 7 Nm could not be exceeded. Premature crack formation in piezoceramics before optimum torque value was reached may be related to the non-uniform stress distribution in the

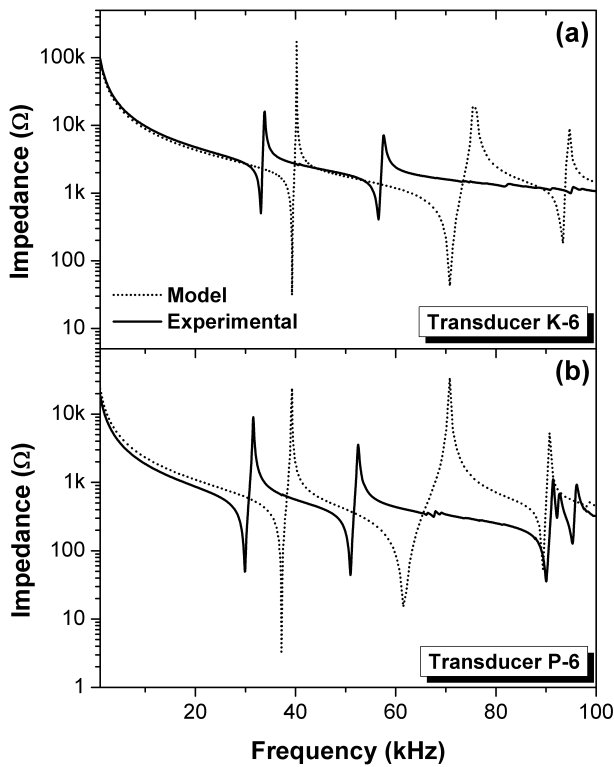


Figure 6. Comparison of simulated and experimentally measured impedance-frequency spectra of BLTs - lead-free K-6 (a) and lead-based P-6 (b)

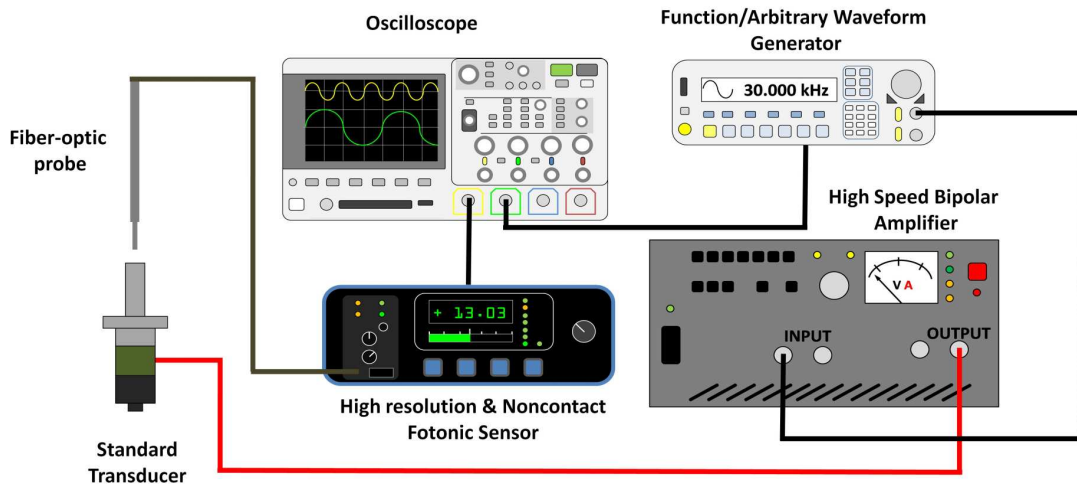


Figure 7. The displacement measurement system at the tip of the horn at working frequency of BLTs

individual ceramics rings due to the lack of perfect parallelism of ceramic rings. Therefore, unfortunately a perfect match, like the one shown in Fig. 1b, between experimentally found and simulated fundamental impedance peaks of BLTs could not be achieved in this study. However, the obtained results were a good guide for the transducer design.

Transducer characterizations were done by measuring the displacements at the tip of the horn at working resonance frequencies using the system as shown in Fig. 7. In the same figure, devices and their connections were shown in detail, as well. With the shown setup, non-contact displacement measurements could be done up to 150 kHz in high resolution. First, a low peak-to-peak sinusoidal voltage (V_{p-p}) waveform was created via a function generator and then it was amplified by using a high frequency power amplifier. The applied high V_{p-p} voltage ranging from 40 V to 100 V was used to drive the K-6 or P-6 transducers. Meanwhile, voltage versus time data from photonic sensor were recorded by an oscilloscope together with the applied sinusoidal waveform, simultaneously. Finally, the peak-to-peak displacements (x_{p-p}) in μm were calculated by multiplying the voltage data by the calibration constant of the used fiber-optic probe.

Figure 8 shows the x_{p-p} vs. time graphs of K-6 and P-6 transducers driven between 40 and 100 V peak-to-peak voltages. It was found that the x_{p-p} values at the tip of the horns increased with increasing amplification

level. The measured x_{p-p} at the tip of the horn at 100 V reached 45.6 μm and 67.8 μm for K-6 and P-6 transducers, respectively. The x_{p-p} value of PZT based transducer was higher than that of KNN based one as expected. This experimental finding is consistent with the result of FEA. On the other hand, it was found that the dependency of peak-to-peak displacement of K6 transducer on the driving potential level was stronger than that of P6 ones.

For instance, the ratio of measured x_{p-p} of K-6 to that of P-6 transducer was found to be approximately 0.4, 0.5, 0.6 and 0.7 at 40 V, 60 V, 80 V and 100 V, respectively. However, in simulation it was assumed that displacement was proportional to the magnitude of the electrical potential. So, discrepancy between experimental and simulation results may be related to nonlinearities observed in piezoelectric materials [80]. Compared to both soft and hard PZT transducers, lead-free CuO doped KNN transducers with smaller nonlinear coefficients were reported to exhibit a better voltage stability [88]. Besides, internal heating of P-6 transducer due to the electrical losses was relatively higher as compared to K-6 transducer when driven continuously, especially at high voltages. That was probably due to the better thermal stability of KNN-KCN piezoceramics than that of hard PZT [26,54]. Generally speaking, the power dissipation in the form of temperature rise during operation was one of the main reasons of transducer failures at high duty cycles [89]. Therefore, it is suggested that long-term performance of transducers under various conditions, such as mechanical stress, driving electric fields etc. should be studied as well as at different working temperatures.

Figure 9 compares fundamental impedance peaks of the K-6 lead-free BLT and the ultrasonic cutting device with and without attached blade. It was observed that the fundamental resonance frequency of the K-6 transducer with bare horn shifted from 33.1 kHz to 34.4 kHz in the presence of a vertical groove and a screw hole. Conversely, the fundamental resonance frequency of the

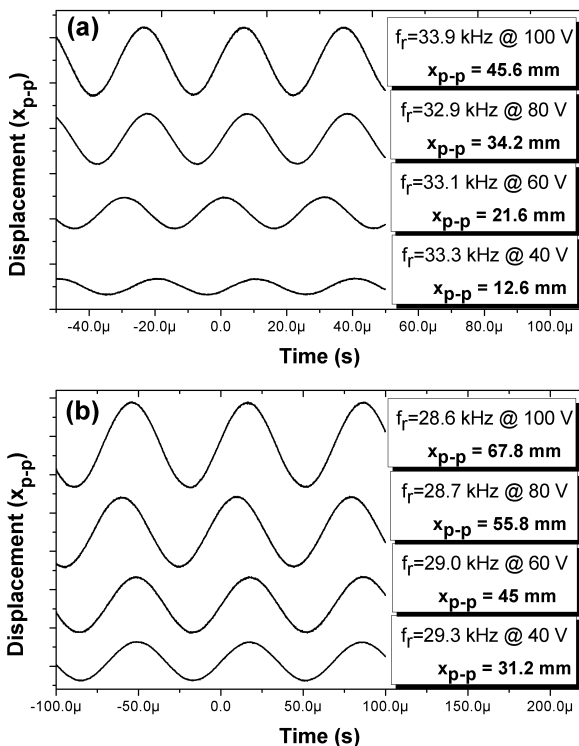


Figure 8. Peak-to-peak displacement (x_{p-p}) vs. time measured from the tip of the horns of BLTs under various driving potential differences - lead-free K-6 (a), lead-based P-6 (b)

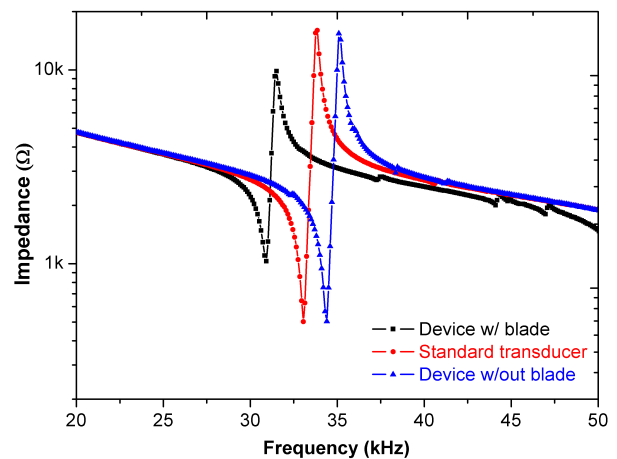


Figure 9. Fundamental impedance peaks of K-6 lead-free BLT, ultrasonic cutting device with and without a blade

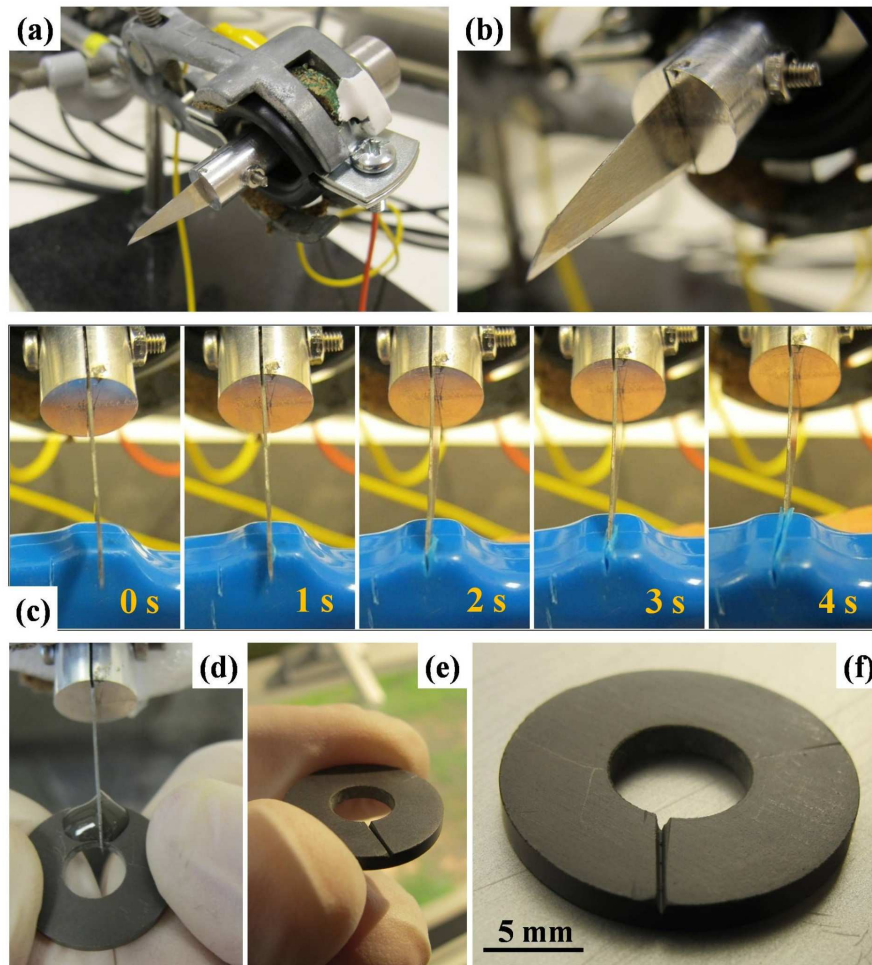


Figure 10. Applications of prototype ultrasonic cutting device made from KNN-KCN-ZnSn piezoceramics: device and holder (a), close-up view of blade attached to the tip of horn (b), frames taken during plastic cutting (c), ultrasonic cutting of PZT-4 piezoceramic ring with diamond abrasives (d), general view of ceramic ring after cutting (e), ceramic ring after being ultrasonically cut (f)

ultrasonic cutting device shifted to 30.95 kHz when a cutting blade was clamped to the tip of the horn together with a clamping bolt, nut and washer. A decrease or increase in total mass of the device was responsible for the shifting of the resonance frequency [90]. Meanwhile, spurious resonance peaks observed at frequencies above 37.5 kHz from ultrasonic cutting device with a clamped blade were probably due to the clamping of the blade by bolt, nut and washer. Fortunately, the fundamental peak of the device was clear and far from those spurious peaks.

As a demonstration, ultrasonic cutting of plastic and ceramic materials was carried out using a lead-free KNN-KCN-ZnSn based prototype device which was driven at 30.5 kHz sinusoidal wave whose peak-to-peak voltage was $V_{p-p} = 150$ V. Experimental setup showing how the ultrasonic cutting was done is shown in Fig. 10a,b. The device was held as its flange on the horn by a rubber lined Munsen ring. The frames captured in the first four seconds of plastic cutting were shown in Fig. 10c. A piece of thermoplastic material (polystyrene) 2 cm wide was cut in a short time period due to the high-frequency vibration in the blade. Relatively low vi-

bration amplitude was created when a high-frequency AC electric field was applied to a piezoceramic stack. However, Langevin type bolt-clamped transducers were not only magnifying vibration amplitudes but also effectively transferring it to the blade.

Owing to the axial oscillation of the blade (theoretically $\sim 30,000$ times per second), local melting took place at the contact regions between the vibrating blade and thermoplastic material. Therefore, the cutting process was quickly and easily accomplished without the need for an extra force. Conventional cutting of plastic material with a craft knife was a difficult task compared to cutting with the ultrasonic cutter. Video showing the ultrasonic cutting of the plastic material is given as Supplementary material (Video 1[§]).

Ultrasonic cutting of a notch on a PZT4 ceramic ring was also done. To speed up the cutting process a relatively soft ceramic was chosen. Diamond polishing suspension (Leco, LE 811-504-008) was used to ease the cutting process (see Fig. 10d). Ceramic cutting with the ultrasonic cutting device is given as Supplementary material (Video 2[†]). General and close-up images of notched PZT4 ceramic rings after about 2 min-

utes of cutting were shown in Fig. 10e,f. Even though the cutting of the ceramics was proceeded without any problem with the craft knife, it is suggested that a harder blade would give a better cutting performance. All these results demonstrate that lead-free KNN-KCN based piezoceramics could be used as active elements for high-power ultrasonic cutting applications instead of lead-based PZT counterparts. Especially, ZnO + SnO₂ co-doped KNN-KCN piezoceramics are potential lead-free piezoelectric candidates to be used in high power applications due to their hard piezoelectric properties.

V. Conclusions

Modelling, fabrication and characterization of eco-friendly hard lead-free KNN piezoceramics based BLT for high-power ultrasonic cutting prototype device were done for the first time in this study. In this respect, dense KNN-KCN piezoceramics were sintered at lower temperatures by Zn,Sn co-doping. Moreover, hard piezoelectric properties required for high-power applications of KNN-KCN piezoceramics were enhanced in the presence of ZnO and SnO₂. The electrical and mechanical losses in the undoped KNN-KCN were low with Zn²⁺ and Sn⁴⁺ ions as well as Cu²⁺ ions doping probably due to the formation of more oxygen vacancies, V_O^{••}. In addition, Zn,Sn co-doped KNN-KCN piezoceramics were found to have comparable high-power characteristics and even better thermal stability than those of hard PZT ones. Lead-free and lead-based BLTs with working frequencies between 30 and 40 kHz were designed via ATILA FEA software and then a prototype BLT was made for the ultrasonic cutting process. Both simulated and experimentally measured results showed that the longitudinal displacement, at ~30 kHz at the tip of the horn of a BLT made from lead-free KNN-KCN-ZnSn piezoceramics, was comparable to that of a PZT4 based BLT. Then, the prototype BLT was further modified to be an ultrasonic cutting device. The cutting performance on the plastic and ceramic materials was tested qualitatively. It was confirmed that KNN-KCN-ZnSn piezoceramics were good lead-free active elements alternative to lead-based PZT counterparts for high-power BLT ultrasonic applications. In conclusion, the novelty of this study was the fabrication and characterization of a working prototype that can be used as an ultrasonic cutting device made from compositionally modified hard lead-free KNN-KCN piezoceramics and finite element modelling of it.

Acknowledgement: This work was supported by Gebze Technical University (formerly GYTE) Scientific Research Projects (BAP) [grant numbers: GYTE-2014-A-22 and GYTE-2013-A-27].

§ Video 1 can be downloaded using following link: <https://goo.gl/3gwmZo>

† Video 2 can be downloaded using following link: <https://goo.gl/a5Vn9R>

References

1. J. Rödel, K.G. Webber, R. Dittmer, W. Jo, M. Kimura, D. Damjanovic, “Transferring lead-free piezoelectric ceramics into application”, *J. Eur. Ceram. Soc.*, **35** [6] (2015) 1659–1681.
2. J.F. Li, K. Wang, F.Y. Zhu, L.Q. Cheng, F.Z. Yao, “(K,Na)NbO₃-based lead-free piezoceramics: Fundamental aspects, processing technologies, and remaining challenges”, *J. Am. Ceram. Soc.*, **96** [12] (2013) 3677–3696.
3. C.H. Hong, H.P. Kim, B.Y. Choi, H.S. Han, J.S. Son, C.W. Ahn, W. Jo, “Lead-free piezoceramics - Where to move on?”, *J. Materiomics*, **2** [1] (2016) 1–24.
4. Restriction of the Use of Certain Hazardous Substances in Electrical and Electronic Equipment (RoHS), *Directive 2002/95/EC of the European Parliament and of the Council*, 2003.
5. Y. Saito, H. Takao, T. Tani, T. Nonoyama, K. Takatori, T. Homma, T. Nagaya, M. Nakamura, “Lead-free piezoceramics”, *Nature*, **432** [7013] (2004) 84–87.
6. T. Tou, Y. Hamaguti, Y. Maida, H. Yamamori, K. Takahashi, Y. Terashima, “Properties of (Bi_{0.5}Na_{0.5})TiO₃-BaTiO₃-(Bi_{0.5}Na_{0.5})(Mn_{1/3}Nb_{2/3})O₃ lead-free piezoelectric ceramics and its application to ultrasonic cleaner”, *Jpn. J. Appl. Phys.*, **48** (2009) 07GM03.
7. T.J. Mason, D. Peters, “An introduction to the uses of power ultrasound in chemistry”, pp. 1–48 in *Practical Sonochemistry: Power Ultrasound Uses and Applications*. Eds. T.J. Mason, D. Peters, Woodhead Publishing, Cambridge, UK, 2002.
8. A. Shoh, “Industrial applications of ultrasound - A review I. high-power ultrasound”, *IEEE Trans. Sonics Ultrason.*, **22** [2] (1975) 60–70.
9. X. Bao, Y. Bar-Cohen, Z. Chang, B.P. Dolgin, S. Sherrit, D.S. Pal, S. Du, T. Peterson, “Modeling and computer simulation of ultrasonic/sonic driller/corer (USDC)”, *IEEE Trans. Ultrason. Ferroelectr. Freq. Control.*, **50** [9] (2003) 1147–1160.
10. A. Cardoni, M. Lucas, M. Cartmell, F. Lim, “A novel multiple blade ultrasonic cutting device”, *Ultrasonics*, **42** (2004) 69–74.
11. P.W.P. Chu, H.L. Li, H.L.W. Chan, K.M.W. Ng, P.C.K. Liu, “Smart ultrasonic transducer for wire-bonding applications”, *Mater. Chem. Phys.*, **75** [1-3] (2002) 95–100.
12. B.J. O’Daly, E. Morris, G.P. Gavin, J.M. O’Byrne, G.B. McGuinness, “High-power low-frequency ultrasound: A review of tissue dissection and ablation in medicine and surgery”, *J. Mater. Process. Technol.*, **200** [1-3] (2008) 38–58.
13. K.S. Suslick, “Sonochemistry”, *Science*, **247** [4949] (1990) 1439–1445.
14. T.B. Thoe, D.K. Aspinwall, M.L.H. Wise, “Review on ultrasonic machining”, *Int. J. Mach. Tools Manuf.*, **38** [4] (1998) 239–255.
15. X. Xian, S. Lin, “Study on the compound multifrequency ultrasonic transducer in flexural vibration”, *Ultrasonics*, **48** [3] (2008) 202–208.
16. Z. Zhang, V.I. Babitsky, “Finite element modeling of a micro-drill and experiments on high speed ultrasonically assisted micro-drilling”, *J. Sound Vib.*, **330** [10] (2011) 2124–2137.
17. H.L. Li, C.P. Chong, H.L.W. Chan, P.C.K. Liu, “Finite element analysis on 1-3 piezocomposite rings for ultrasonic transducer applications”, *Ceram. Int.*, **30** [7] (2004) 1827–

- 1830.
18. L. Shuyu, “Load characteristics of high power sandwich piezoelectric ultrasonic transducers”, *Ultrasonics*, **43** [5] (2005) 365–373.
 19. T.H. Yan, W. Wang, X.D. Chen, Q. Li, C. Xu, “Design of a smart ultrasonic transducer for interconnecting machine applications”, *Sensors*, **9** [6] (2009) 4986–5000.
 20. H.L.W. Chan, S.H. Choy, C.P. Chong, H.L. Li, P.C.K. Liu, “Bismuth sodium titanate based lead-free ultrasonic transducer for microelectronics wirebonding applications”, *Ceram. Int.*, **34** [4] (2008) 773–777.
 21. S.H. Choy, X.X. Wang, C.P. Chong, H.L.W. Chan, P.C.K. Liu, C.L. Choy, “0.90(Bi_{1/2}Na_{1/2})TiO₃-0.05(Bi_{1/2}K_{1/2})TiO₃-0.05BaTiO₃ transducer for ultrasonic wirebonding applications”, *Appl. Phys. A*, **84** [3] (2006) 313–316.
 22. K.W. Kwok, T. Lee, S.H. Choy, H.L.W. Chan, “Lead-free piezoelectric transducers for microelectronic wirebonding applications”, pp. 145–164 in *Piezoelectric Ceramics*. Eds. E. Suaste-Gomez, Sciyo, Rijeka, 2010.
 23. T. Lee, *Development of Lead-free Ultrasonic Wirebonding Transducers for Microelectronic Packaging Applications*, M. Phil. Thesis, Hong Kong Polytechnic University, Hong Kong, 2008.
 24. T. Lee, K.W. Kwok, H.L. Li, H.L.W. Chan, “Lead-free alkaline niobate-based transducer for ultrasonic wirebonding applications”, *Sens. Actuaors. A: Phys.*, **150** [2] (2009) 267–271.
 25. T.R. Shrout, S.J. Zhang, “Lead-free piezoelectric ceramics: Alternatives for PZT?”, *J. Electroceram.*, **19** [1] (2007) 113–126.
 26. S. Zhang, J.B. Lim, H.J. Lee, T.R. Shrout, “Characterization of hard piezoelectric lead-free ceramics”, *IEEE Trans. Ultrason. Ferroelectr. Freq. Control.*, **56** [8] (2009) 1523–1527.
 27. D.A. Berlincourt, D.R. Curran, H. Jaffe, “Piezoelectric and piezomagnetic materials and their function in transducers”, pp. 170–267 in *Physical Acoustics: Principles and Methods*. Eds. W.P. Mason, Academic Press, New York, 1964.
 28. H.J. Lee, S.O. Ural, L. Chen, K. Uchino, S. Zhang, “High power characteristics of lead-free piezoelectric ceramics”, *J. Am. Ceram. Soc.*, **95** [11] (2012) 3383–3386.
 29. K. Uchino, *Ferroelectric Devices*, Marcel Dekker, New York 2000.
 30. J. Bernard, A. Benčan, T. Rojac, J. Holc, B. Malič, M. Kosec, “Low-temperature sintering of K_{0.5}Na_{0.5}NbO₃ ceramics”, *J. Am. Ceram. Soc.*, **91** [7] (2008) 2409–2411.
 31. Y. Guo, K. Kakimoto, H. Ohsato, “Dielectric and piezoelectric properties of lead-free (Na_{0.5}K_{0.5})NbO₃-SrTiO₃ ceramics”, *Solid. State Commun.*, **129** [5] (2004) 279–284.
 32. Z. Li, G. Xu, Y. Li, A. Sun, L. Duan, J. Jiang, P. Cui, “Dielectric and piezoelectric properties of ZnO and SnO₂ co-doping K_{0.5}Na_{0.5}NbO₃ ceramics”, *Physica B*, **405** [1] (2010) 296–299.
 33. D. Lin, K.W. Kwok, H.L.W. Chan, “Piezoelectric and ferroelectric properties of Cu-doped K_{0.5}Na_{0.5}NbO₃ lead-free ceramics”, *J. Phys. D*, **41** [4] (2008) 045401.
 34. H.Y. Park, I.T. Seo, J.H. Choi, S. Nahm, H.G. Lee, “Low-temperature sintering and piezoelectric properties of (Na_{0.5}K_{0.5})NbO₃ lead-free piezoelectric ceramics”, *J. Am. Ceram. Soc.*, **93** [1] (2010) 36–39.
 35. S.H. Park, C.W. Ahn, S. Nahm, J.S. Song, “Microstructure and piezoelectric properties of ZnO-added (Na_{0.5}K_{0.5})NbO₃ ceramics”, *Jpn. J. Appl. Phys.*, **43** [8B] (2004) L1072.
 36. I.T. Seo, H.Y. Park, N.V. Dung, M.K. Choi, S. Nahm, H.G. Lee, B.H. Choi, “Microstructure and piezoelectric properties of (Na_{0.5}K_{0.5})NbO₃ lead-free piezoelectric ceramics with V₂O₅ addition”, *IEEE Trans. Ultrason. Ferroelectr. Freq. Control.*, **56** [11] (2009) 2337–2342.
 37. K. Wang, J.F. Li, N. Liu, “Piezoelectric properties of low-temperature sintered Li-modified (Na,K)NbO₃ lead-free ceramics”, *Appl. Phys. Lett.*, **93** [9] (2008) 092904.
 38. S.L. Yang, C.C. Tsai, Y.C. Liou, C.S. Hong, B.J. Li, S.Y. Chu, “Investigation of CuO-doped NKN ceramics with high mechanical quality factor synthesized by a B-site oxide precursor method”, *J. Am. Ceram. Soc.*, **95** [3] (2012) 1011–1017.
 39. R. Zuo, J. Rödel, R. Chen, L. Li, “Sintering and electrical properties of lead-free Na_{0.5}K_{0.5}NbO₃ piezoelectric ceramics”, *J. Am. Ceram. Soc.*, **89** [6] (2006) 2010–2015.
 40. A.J. Moulson, J.M. Herbert, *Electroceramics: Materials, Properties, Applications*, John Wiley & Sons, Cornwall, UK 2003.
 41. C.W. Ahn, M. Karmarkar, D. Viehland, D.H. Kang, K.S. Bae, S. Priya, “Low temperature sintering and piezoelectric properties of CuO-doped (K_{0.5}Na_{0.5})NbO₃ ceramics”, *Ferroelectrics Lett.*, **35** [3–4] (2008) 66–72.
 42. E.M. Alkoy, A. Berksoy-Yavuz, “Electrical properties and impedance spectroscopy of pure and copper-oxide-added potassium sodium niobate ceramics”, *IEEE Trans. Ultrason. Ferroelectr. Freq. Control.*, **59** [10] (2012) 2121–2128.
 43. E.M. Alkoy, M. Papila, “Microstructural features and electrical properties of copper oxide added potassium sodium niobate ceramics”, *Ceram. Int.*, **36** [6] (2010) 1921–1927.
 44. F. Azough, M. Wegrzyn, R. Freer, S. Sharma, D. Hall, “Microstructure and piezoelectric properties of CuO added (K,Na,Li)NbO₃ lead-free piezoelectric ceramics”, *J. Eur. Ceram. Soc.*, **31** [4] (2011) 569–576.
 45. E. Li, H. Kakimoto, S. Wada, T. Tsurum, “Influence of CuO on the structure and piezoelectric properties of the alkaline niobate-based lead-free ceramics”, *J. Am. Ceram. Soc.*, **90** [6] (2007) 1787–1791.
 46. J.B. Lim, Y.H. Jeong, M.H. Kim, D. Suvorov, J.H. Jeon, “Effect of K/Na ratio on piezoelectric properties of modified-(K_{1-x}Na_x)NbO₃ “hard” lead-free piezoelectrics”, *Ceram. Int.*, **38** [3] (2012) 2605–2608.
 47. J.B. Lim, S. Zhang, J.H. Jeon, T.R. Shrout, “(K,Na)NbO₃-based ceramics for piezoelectric “hard” lead-free materials”, *J. Am. Ceram. Soc.*, **93** [5] (2010) 1218–1220.
 48. J.B. Lim, S. Zhang, H.J. Lee, J.H. Jeon, T.R. Shrout, “Shear-mode piezoelectric properties of modified-(K,Na)NbO₃ ceramics for “hard” lead-free materials”, *J. Am. Ceram. Soc.*, **93** [9] (2010) 2519–2521.
 49. D. Lin, K.W. Kwok, H.W.L. Chan, “Dielectric and piezoelectric properties of (K_{0.5}Na_{0.5})NbO₃-Ba(Zr_{0.05}Ti_{0.95})O₃ lead-free ceramics”, *Appl. Phys. Lett.*, **91** [14] (2007) 143513.
 50. S. Su, R. Zuo, Y. Ran, W. Zhao, X. Wang, L. Li, “Microstructure, electrical properties and processing dependence of CuO modified (Na_{0.52}K_{0.48})NbO₃ ceramics”, *Ceram. Silik.*, **54** [4] (2010) 320–324.
 51. C.C. Tsai, S.Y. Chu, C.S. Hong, S.L. Yang, “Influence of A-site deficiency on oxygen-vacancy-related dielectric re-

- laxation, electrical and temperature stability properties of CuO-doped NKN-based piezoelectric ceramics”, *Ceram. Int.*, **39** (2013) S165–S170.
52. R. Wang, S. Shibusawa, N. Miura, H. Bando, M. Itoh, “Fabrication and characterization of niobate piezoelectric ceramics with sintering aids”, *Ferroelectrics*, **385** [1] (2009) 6141–6148.
 53. Q. Chen, L. Chen, Q. Li, X. Yue, D. Xiao, J. Zhu, X. Shi, Z. Liu, “Piezoelectric properties of $K_4CuNb_8O_{23}$ modified $(Na_{0.5}K_{0.5})NbO_3$ lead-free piezoceramics”, *J. Appl. Phys.*, **102** [10] (2007) 104109.
 54. Q. Chen, Y. Chen, Z. Peng, J. Wu, H. Liu, D. Xiao, P. Yu, J. Zhu, J. Zhu, “Temperature dependent properties and poling effect of $K_4CuNb_8O_{23}$ modified $(Na_{0.5}K_{0.5})NbO_3$ lead free piezoceramics”, *J. Appl. Phys.*, **117** [12] (2015) 124103.
 55. J. Hao, Z. Xu, R. Chu, Y. Zhang, Q. Chen, G. Li, Q. Yin, “Enhanced temperature stability of modified $(K_{0.5}Na_{0.5})_{0.94}Li_{0.06}NbO_3$ lead-free piezoelectric ceramics”, *J. Mater. Sci.*, **44** [22] (2009) 6162–6166.
 56. J. Hao, Z. Xu, R. Chu, Y. Zhang, G. Li, Q. Yin, “Effects of $K_4CuNb_8O_{23}$ on the structure and electrical properties of lead-free $0.94(Na_{0.5}K_{0.5})NbO_3-0.06LiNbO_3$ ceramics”, *Mater. Res. Bull.*, **44** [10] (2009) 1963–1967.
 57. S.H. Lee, K.S. Lee, J.H. Yoo, Y.H. Jeong, H.S. Yoon, “Dielectric and piezoelectric properties of $(K_{0.5}Na_{0.5})(Nb_{0.97}Sb_{0.03})O_3$ ceramics doped with $K_4CuNb_8O_{23}$ ”, *Trans. Electr. Electron. Mater.*, **12** [2] (2011) 72–75.
 58. Y. Liu, R. Chu, Z. Xu, H. Lv, L. Wu, Y. Yang, G. Li, “Effects of $K_4CuNb_8O_{23}$ on phase structure and electrical properties of $K_{0.5}Na_{0.5}NbO_3-LiSbO_3$ lead-free piezoceramics”, *Physica B*, **407** [13] (2012) 2573–2577.
 59. Y.G. Lv, C.L. Wang, J.L. Zhang, M.L. Zhao, M.K. Li, H.C. Wang, “Modified $(K_{0.5}Na_{0.5})(Nb_{0.9}Ta_{0.1})O_3$ ceramics with high Q_m ”, *Mater. Lett.*, **62** [19] (2008) 3425–3427.
 60. M. Matsubara, T. Yamaguchi, K. Kikuta, S. Hirano, “Sinterability and piezoelectric properties of $(K,Na)NbO_3$ ceramics with novel sintering aid”, *Jpn. J. Appl. Phys.*, **43** [10] (2004) 7159–7163.
 61. M. Matsubara, T. Yamaguchi, W. Sakamoto, K. Kikuta, T. Yogo, S. Hirano, “Processing and piezoelectric properties of lead-free $(K,Na)(Nb,Ta)O_3$ ceramics”, *J. Am. Ceram. Soc.*, **88** [5] (2005) 1190–1196.
 62. B. Seo, J. Yoo, “Effect of $K_4CuNb_8O_{23}$ and ZnO on the dielectric and piezoelectric properties of $(K_{0.5}Na_{0.5})NbO_3$ ceramics”, *J. Korean Phys. Soc.*, **57** [4] (2010) 967–970.
 63. J. Yoo, B. Seo, “Dielectric and piezoelectric properties of $(K_{0.5}Na_{0.5})(Nb_{0.96}Sb_{0.04})O_3$ ceramics doped with La_2O_3 ”, *Ferroelectrics*, **425** [1] (2011) 106–113.
 64. J.R. Yoon, C.B. Lee, K.M. Lee, H.Y. Lee, S.W. Lee, “The piezoelectric properties of $(Na_{0.5}K_{0.5})NbO_3-K_4CuNb_8O_{23}$ ceramics with various $K_4CuNb_8O_{23}$ doping and sintering temperatures”, *Trans. Electr. Electron. Mater.*, **11** [3] (2010) 126–129.
 65. E. Akça, *Modification of KNN Ferroelectric Ceramics for High Power Ultrasonic Applications*, Ph.D. Dissertation, Gebze Technical University, Kocaeli, Turkey, 2016.
 66. E. Akça, H. Yılmaz, “Sintering behavior and electrical properties of $K_4CuNb_8O_{23}$ modified $K_{0.5}Na_{0.5}NbO_3$ ceramics with SnO_2 , ZnO or Yb_2O_3 doping”, *Ceram. Int.*, **41** [3] (2015) 3659–3667.
 67. IEEE Standard on Piezoelectricity, in *ANSI/IEEE Std. 176-1987*, pp. 0-1 (1988), doi: 10.1109/IEEESTD.1988.79638.
 68. W. Cao, S. Zhu, B. Jiang, “Analysis of shear modes in a piezoelectric vibrator”, *J. Appl. Phys.*, **83** [8] (1998) 4415–4420.
 69. K. Uchino, J.C. Debus, *Applications of ATILA FEM software to smart materials: Case studies in designing devices*, Woodhead Publishing Limited, Cambridge, UK 2012.
 70. K. Uchino, *FEM and Micromechanics with ATILA Software*, CRC Press, Boca Raton, FL 2008.
 71. S. Su, R. Zuo, X. Wang, L. Li, “Sintering, microstructure and piezoelectric properties of CuO and SnO_2 co-modified sodium potassium niobate ceramics”, *Mater. Res. Bull.*, **45** [2] (2010) 124–128.
 72. K. Carl, K.H. Hardtl, “Electrical after-effects in $Pb(Ti,Zr)O_3$ ceramics”, *Ferroelectrics*, **17** [1] (1977) 473–486.
 73. R.D. Shannon, “Revised effective ionic radii and systematic studies of interatomic distances in halides and chalcogenides”, *Acta Crystallogr.*, **A32** (1976) 751–767.
 74. N. Marandian-Hagh, K. Kerman, B. Jadidian, A. Safari, “Dielectric and piezoelectric properties of Cu^{2+} -doped alkali niobates”, *J. Eur. Ceram. Soc.*, **29** [11] (2009) 2325–2332.
 75. S. Körbel, P. Marton, C. Elsässer, “Formation of vacancies and copper substitutionals in potassium sodium niobate under various processing conditions”, *Phys. Rev. B*, **81** [17] (2010) 174115.
 76. M.J. Hoffmann, H. Kungl, J. Acker, C. Elsässer, S. Körbel, P. Marton, R.A. Eichel, E. Erünal, P. Jakes, “Influence of the A/B stoichiometry on defect structure, sintering, and microstructure in undoped and Cu-doped KNN”, pp. 209–251 in *Lead-Free Piezoelectrics*. Eds. S. Priya, S. Nahm, Springer, New York, 2012.
 77. R.A. Eichel, E. Erünal, P. Jakes, S. Körbel, C. Elsässer, H. Kungl, J. Acker, M.J. Hoffmann, “Interactions of defect complexes and domain walls in CuO-doped ferroelectric $(K,Na)NbO_3$ ”, *Appl. Phys. Lett.*, **102** [24] (2013) 242908.
 78. R.A. Eichel, E. Erünal, M.D. Drahush, D.M. Smyth, J. van Tol, J. Acker, H. Kungl, M.J. Hoffmann, “Local variations in defect polarization and covalent bonding in ferroelectric Cu^{2+} -doped PZT and KNN functional ceramics at the morphotropic phase boundary”, *Phys. Chem. Chem. Phys.*, **11** [39] (2009) 8698–8705.
 79. F.-Z. Yao, K. Wang, J.-F. Li, “Comprehensive investigation of elastic and electrical properties of Li/Ta-modified $(K,Na)NbO_3$ lead-free piezoceramics”, *J. Appl. Phys.*, **113** [17] (2013) 174105.
 80. D.A. Hall, “Review Nonlinearity in piezoelectric ceramics”, *J. Mater. Sci.*, **36** [19] (2001) 4575–4601.
 81. S. Zhang, E.F. Alberta, R.E. Eitel, C.A. Randall, T.R. Shrout, “Elastic, piezoelectric, and dielectric characterization of modified $BiScO_3-PbTiO_3$ ceramics”, *IEEE Trans. Ultrason. Ferroelectr. Freq. Control.*, **52** [11] (2005) 2131–2139.
 82. H. Lee, S. Zhang, Y. Bar-Cohen, S. Sherrit, “High temperature, high power piezoelectric composite transducers”, *Sensors*, **14** [8] (2014) 14526.
 83. H. Nagata, Y. Hiruma, T. Takenaka, “High power piezoelectric characteristics for perovskite-type lead-free ferroelectric ceramics”, *Integr. Ferroelectr.*, **115** [1] (2010) 63–70.
 84. M. Hejazi, E. Taghaddos, E. Gurdal, K. Uchino, A. Sa-

- fari, “High power performance of manganese-doped BNT-based Pb-free piezoelectric ceramics”, *J. Am. Ceram. Soc.*, **97** [10] (2014) 3192–3196.
85. E.A. Gurdal, S.O. Ural, H.Y. Park, S. Nahm, K. Uchino, “High power characterization of $(\text{Na}_{0.5}\text{K}_{0.5})\text{NbO}_3$ based lead-free piezoelectric ceramics”, *Sens. Actuaors. A: Phys.*, **200** (2013) 44–46.
86. W.C. Xu, K.H. Lam, S.H. Choy, H.L.W. Chan, “A stepped horn transducer driven by lead-free piezoelectric ceramics”, *Integr. Ferroelectr.*, **89** [1] (2007) 87–93.
87. H.T. Nguyen, H.D. Nguyen, J.Y. Uan, D.A. Wang, “A nonrational B-spline profiled horn with high displacement amplification for ultrasonic welding”, *Ultrasonics*, **54** [8] (2014) 2063–2071.
88. Y. Liu, T. Morita, “Nonlinear coefficients in lead-free $\text{CuO}-(\text{K},\text{Na})\text{NbO}_3$ transducers”, *Jpn. J. Appl. Phys.*, **54** (2015) 07HC01.
89. J.L. Butler, K.D. Rolt, F.A. Tito, “Piezoelectric ceramic mechanical and electrical stress study”, *J. Acoust. Soc. Am.*, **96** [3] (1994) 1914–1917.
90. D. Ensminger, F.B. Stulen, “Oscillatory Motion and Wave Equations”, pp. 1–25 in *Ultrasonics: Data, Equations and Their Practical Uses*. Eds. D. Ensminger, F.B. Stulen, CRC Press, Boca Raton, FL, 2008.